Supporting Information

Facile Synthesis of Cobalt Clusters-CoN_x Composites: Synergistic Effect Boosts up Electrochemical Oxygen Reduction

Jia Zhang,‡[a] Yan Xie,‡[b], Qike Jiang,[a] Song Guo,*[a] Jiahui Huang,[b] Yue Wang,[c] Liangliang Xu,*[d] Gao Li,*[ae]

a. State Key Laboratory of Catalysis, Dalian Institute of Chemical Physics, Chinese Academy of Sciences, Dalian 116023, China

b. Dalian National Laboratory for Clean Energy, Dalian Institute of Chemical Physics, Chinese Academy of Sciences, Dalian 116023, China

c. Department of Electrical Engineering, Hanyang University, Seoul 04763, Republic of Korea

d. Department of Chemical and Biomolecular Engineering, Korea Advanced Institute of Science and Technology (KAIST), Daejeon 34141, Republic of Korea

e. University of Chinese Academy of Sciences, Beijing 100049, China

‡ J.Z. and Y.X. contributed equally to this work.

E-mail: gaoli@dicp.ac.cn (G.L.), guo_soong@dicp.ac.cn (S.G.), xuliang@kaist.ac.kr (L.X.)

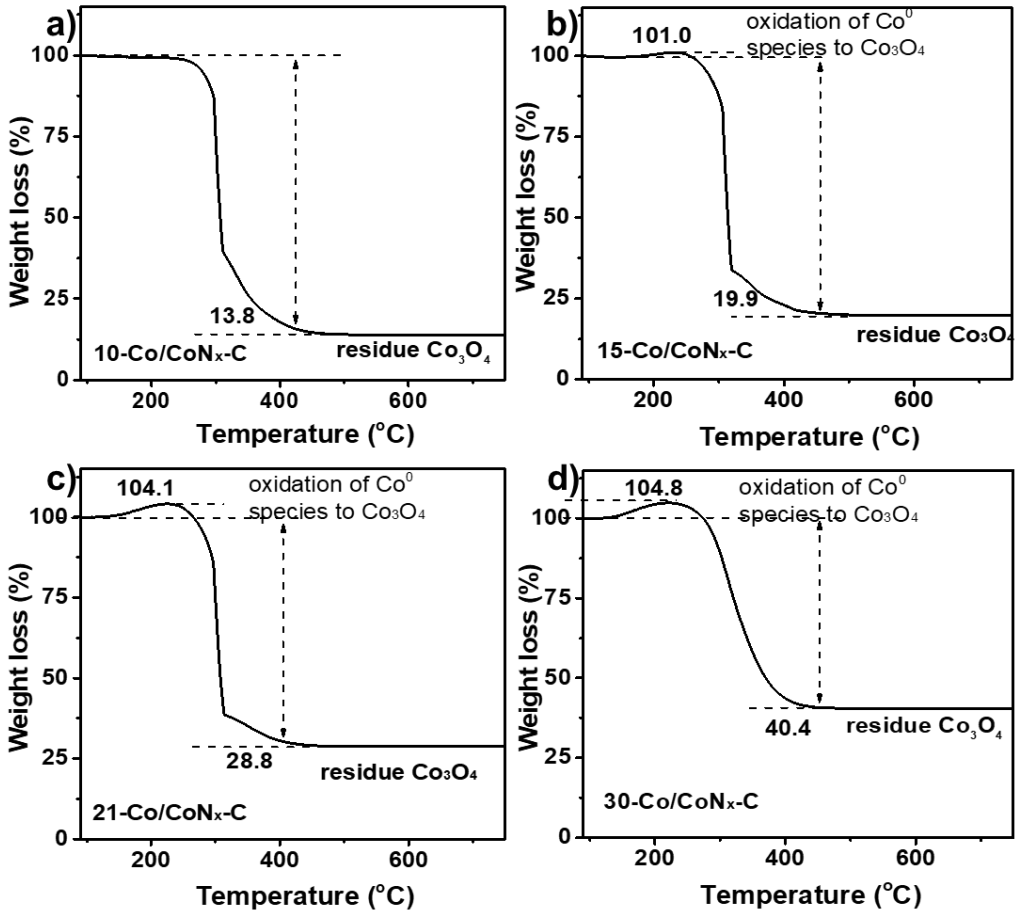

Figure S1. The exact Co content in *x*-Co/CoN_x-C determined by TGA in the presence of air: a) 10-Co/CoN_x-C, b) 15-Co/CoN_x-C, c) 21-Co/CoN_x-C and d) 30-Co/CoN_x-C.

Two steps were observed in these Co/CoN_x-C catalysts with high Co-content (e.g. 15 wt%, 21 wt%, and 30 wt%). The first step with increasing weight at ~ 150 ^oC to ~ 230 ^oC is assigned to the oxidation of the metallic Co nanoparticles (i.e. 3 Co + 2 O_2 → Co_3O_4). And the second step started at ~ 280 ^oC to flat is associated to the combustion of the carbon support and CoN_x species. The final residue is determined to be Co_3O_4 by XRD after the TGA tests at 750 ^oC. Note that CoN_x is main species in the 10-Co/CoN_x-C sample, as the first step is not found in the TGA test.

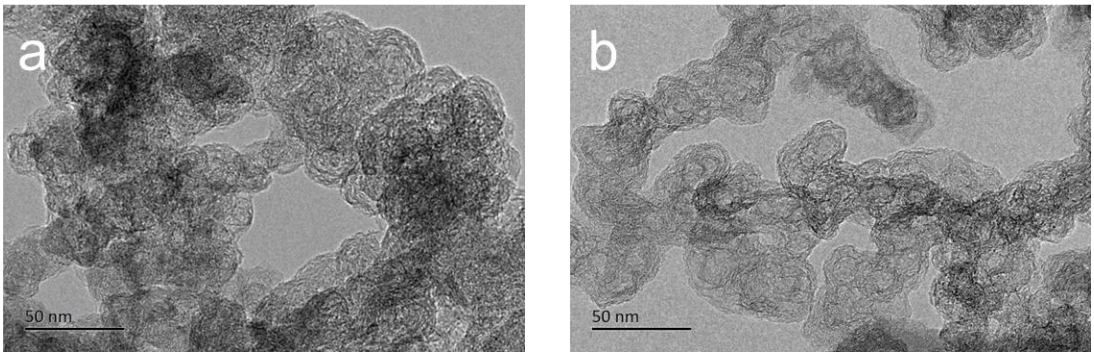

Figure S2. TEM images of 10-Co/CoN_x-C. No clear Co nanoparticles were discernible in TEM, implying that the single-atom CoN_x species is dominated.

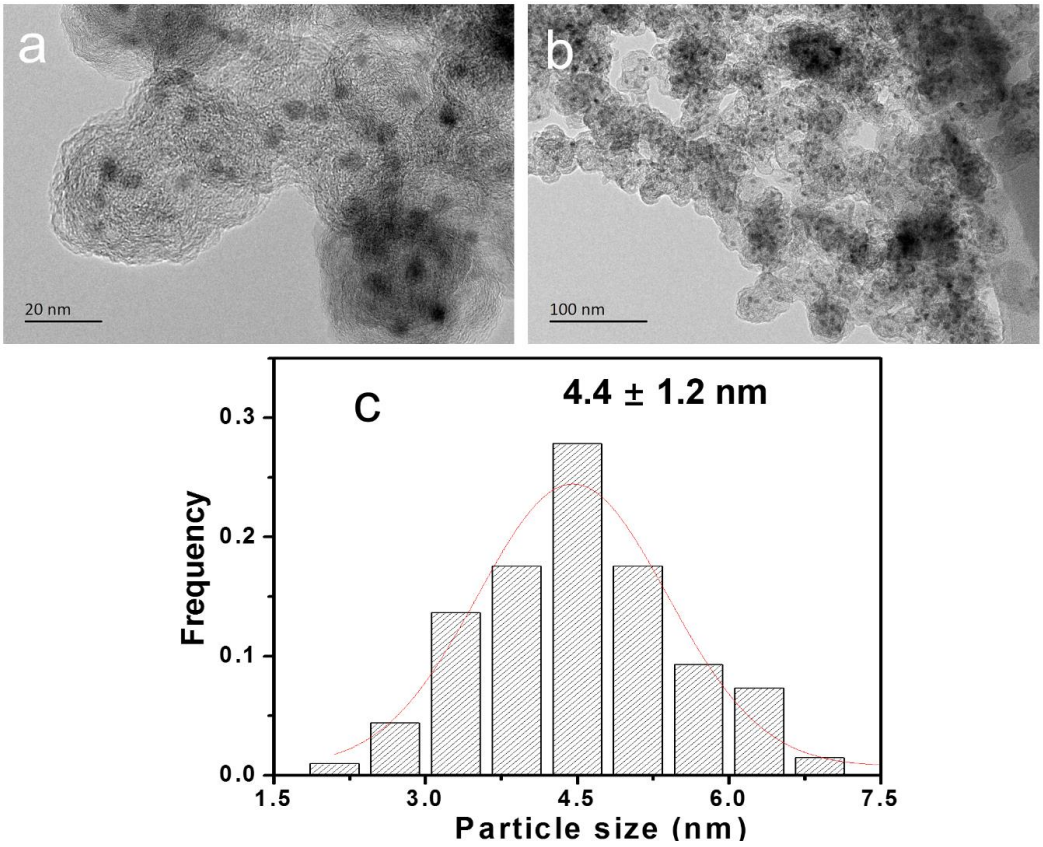

Figure S3. a,b) TEM images of 15-Co/CoN_x-C. c) The size distribution of Co nanoparticles; the size of Co particles is ~ 4.4±1.2 nm. Of note, the single-atom CoN_x species were not counted.

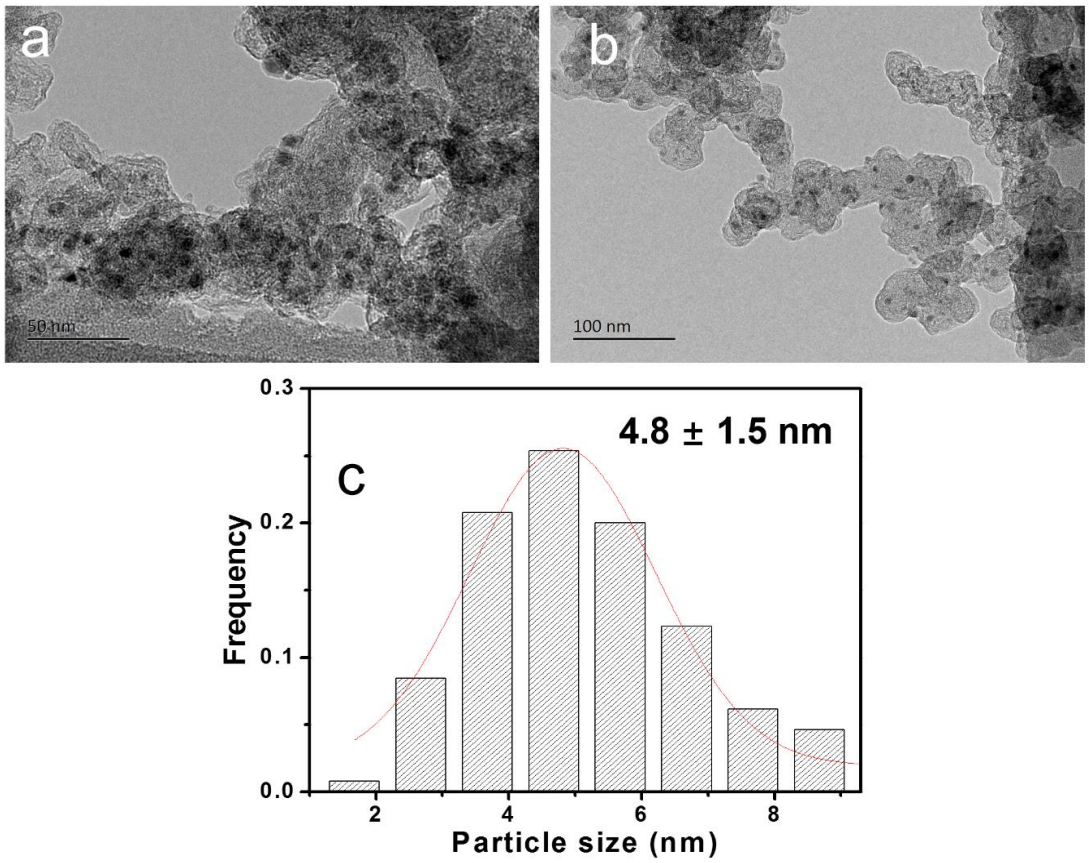

Figure S4. a,b) TEM images of 21-Co/CoN_x-C. c) The size distribution of Co nanoparticles; the size of Co particles is ~ 4.8±1.5 nm. Of note, the single-atom CoN_x species were not counted.

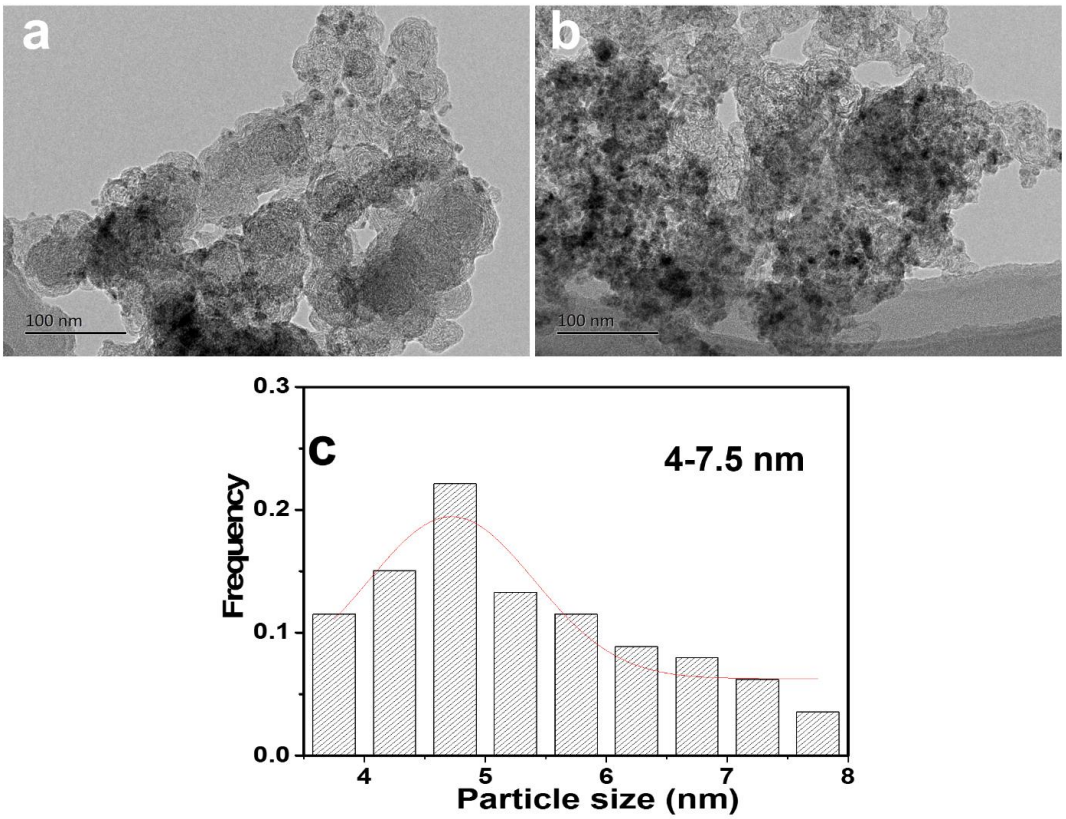

Figure S5. a,b) TEM images of 30-Co/CoN_x-C. c) The size distribution of Co nanoparticles; the size of Co particles is ~ 4-7.5 nm. Of note, the single-atom CoN_x species were not counted.

As shown in the Figures S3-S5, the Co nanoparticles are aggregated to big particles at higher Co concentration under the identical calcination conditions.

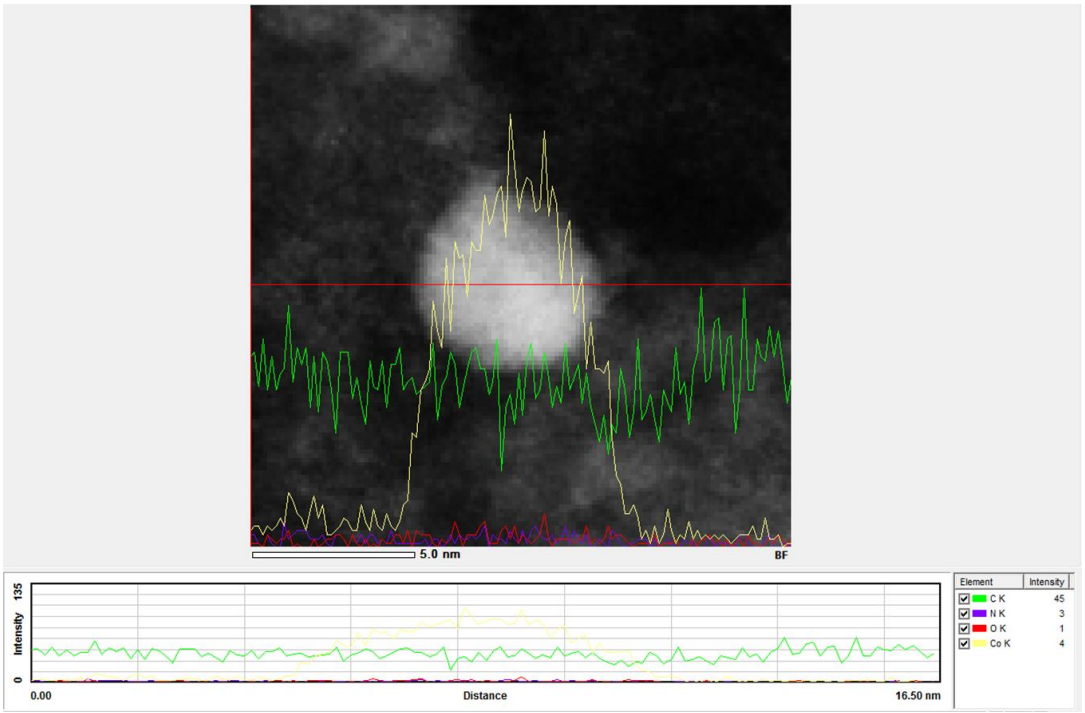

Figure S6. HADDF-STEM images and the corresponding line scanning profiles of 15-Co/CoN_x-C. In the line scanning of the cobalt particle, only the peak assigned to Co was clearly observed and the peaks for N and O were discernible, corroborating that the cobalt particle is metallic, Co^0.

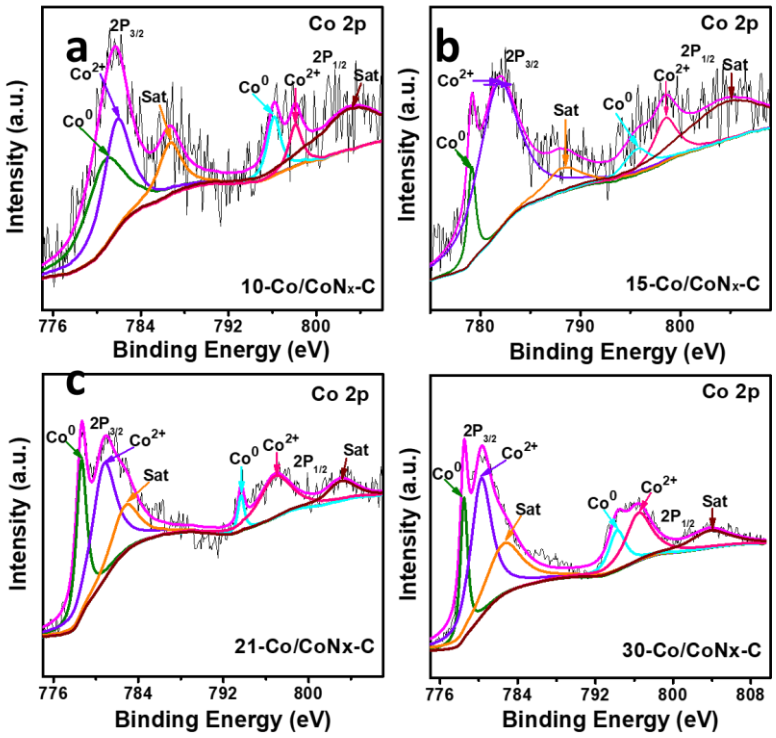

Figure S7. Co 2p XPS spectra of a) 10-Co/CoN$_x$-C, b) 15-Co/CoN$_x$-C, c) 21-Co/CoN$_x$-C, and d) 30-Co/CoN$_x$-C samples.

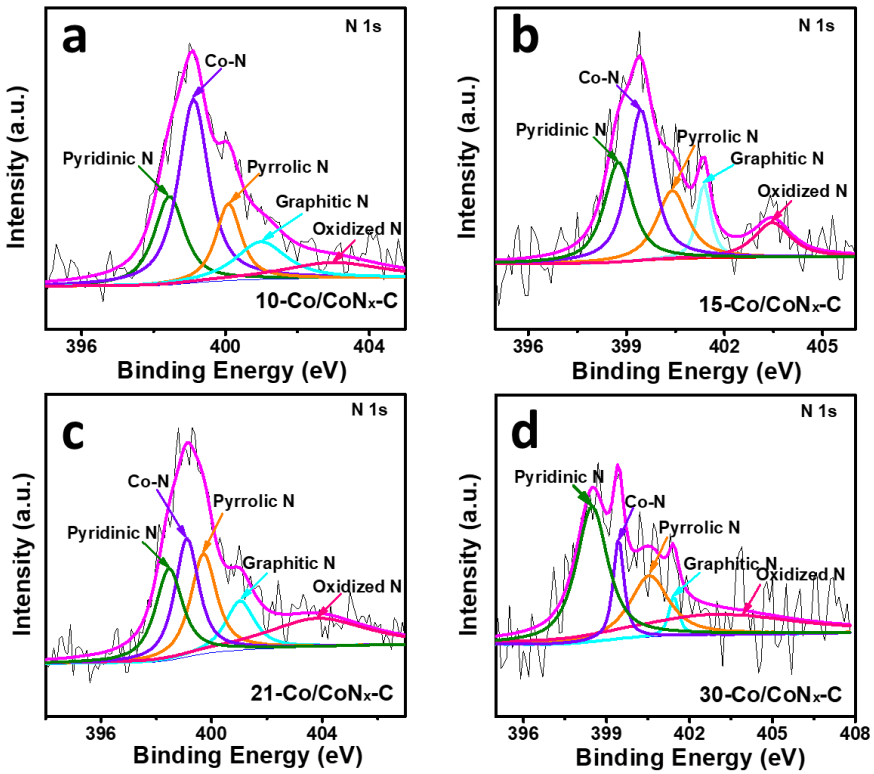

Figure S8. N 1s XPS spectra of a) 10-Co/CoN$_x$-C, b) 15-Co/CoN$_x$-C, c) 21-Co/CoN$_x$-C, and d) 30-Co/CoN$_x$-C samples.

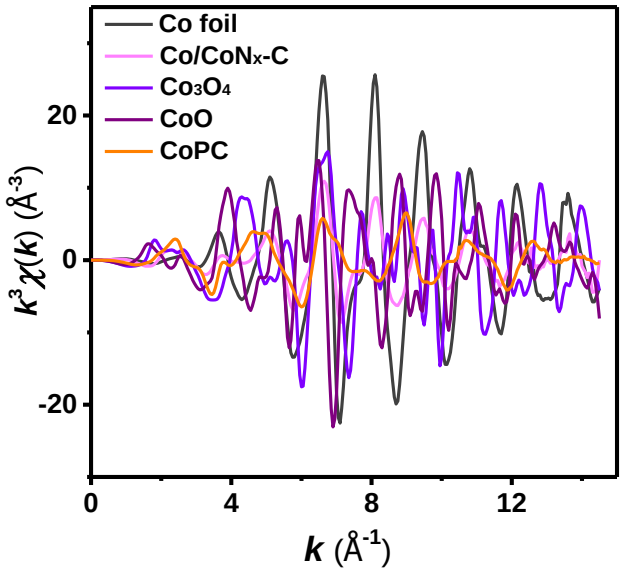

Figure S9. Co K-edge EXAFS oscillation functions $k^3\chi(k)$ (Å^{-3}) of 15-Co/CoN$_x$-C.

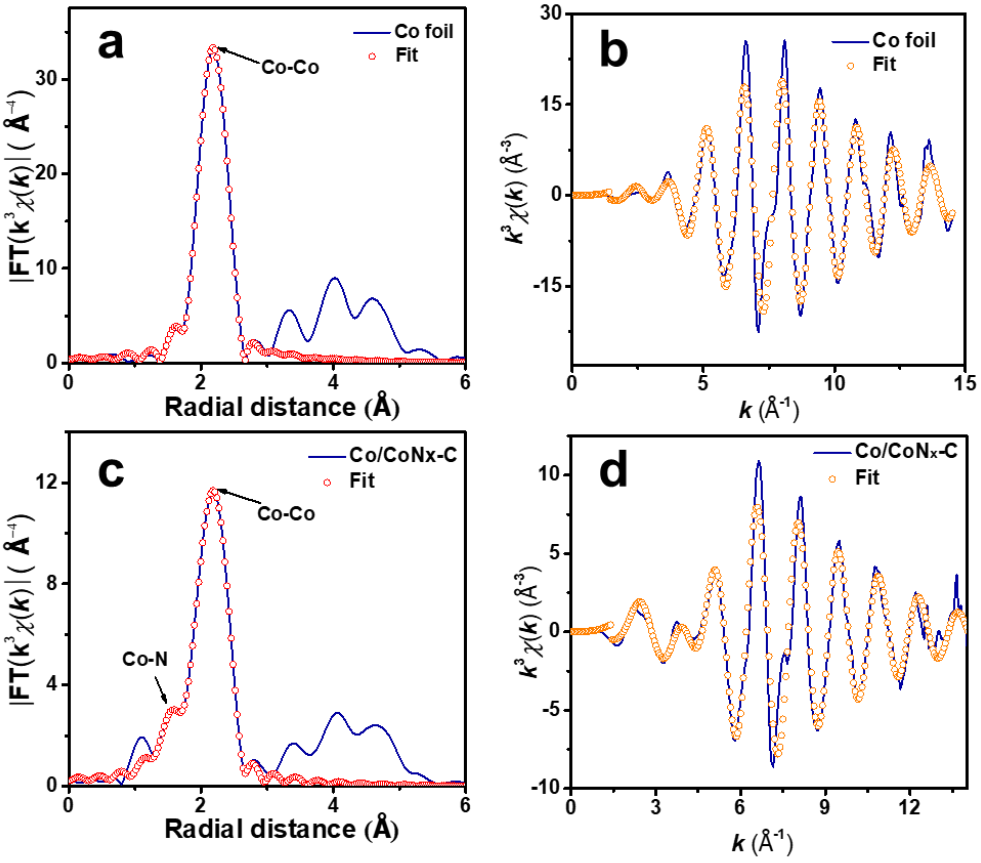

Figure S10. EXAFS fitting curves of Co foil and 15-Co/CoN$_x$-C at the R space (a, c) and k space (b, d), respectively.

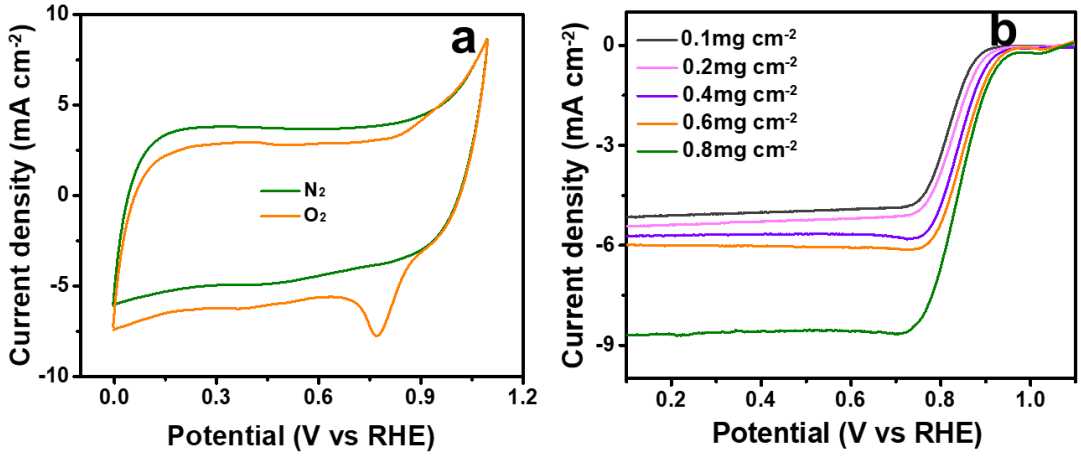

Figure S11. a) CV curves in O_2- and N_2-saturated 0.1M KOH solution of 15-Co/CoN_x-C at 100 mV s^{-1}. b) LSV curves on glassy carbon (GC) by the rotating disk electrode (RDE) at 1600 rpm.

The observation of a reduction peak at around 0.77 V (vs RHE) strongly indicated these electrocatalysts should be effective in ORR. The ORR performances increased with the increasing electrocatalyst loading in the range of 0.1 to 0.6 mg cm^{-2}, while at the high loading of 0.8 mg cm^{-2}, a poor ORR activity was found in terms of the half-wave potential and current density. Thus, electrocatalyst loading of 0.6 mg cm^{-2} was chosen for the further ORR tests.

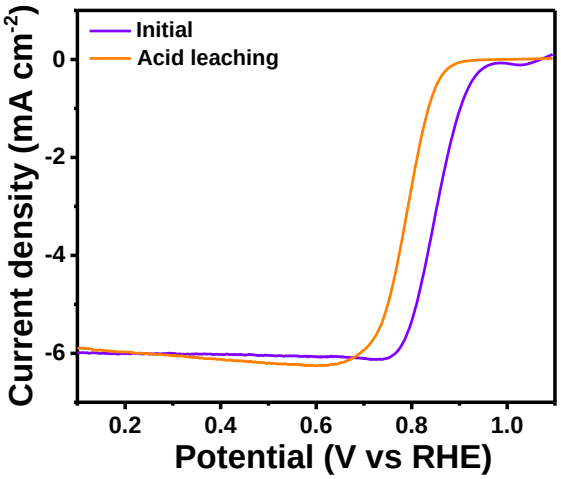

Figure S12. The LSV curves before and after acid leaching of 15-Co/CoN_x-C catalysts. The 15-Co/CoN_x-C samples were treated in a 0.5 M H_2SO_4 solution at 60 ^oC for over 6 h. The metallic Co clusters were removed during the acid leaching.

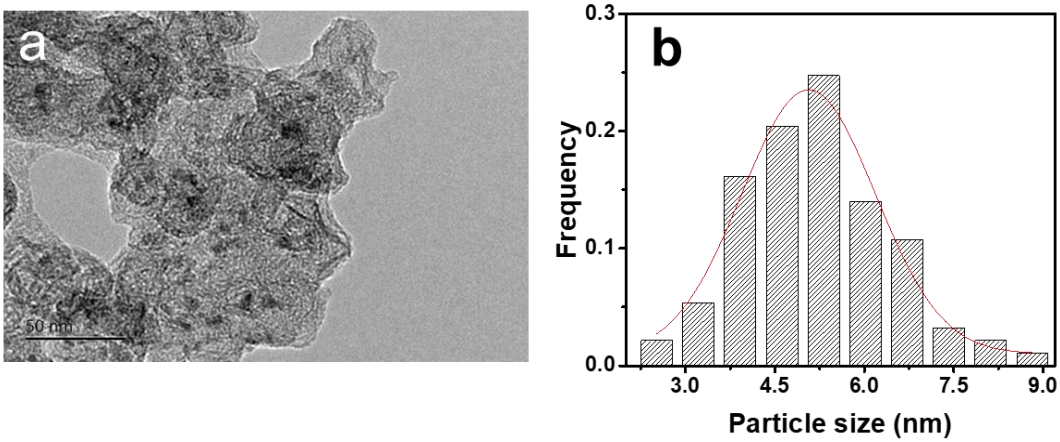

Figure S13. a) TEM image of spent 15-Co/CoNx-C. b) The size distribution of Co nanoparticles; the size of Co particles is ~ 5.0±1.5 nm. Of note, the single-atom CoN_x species were not counted.

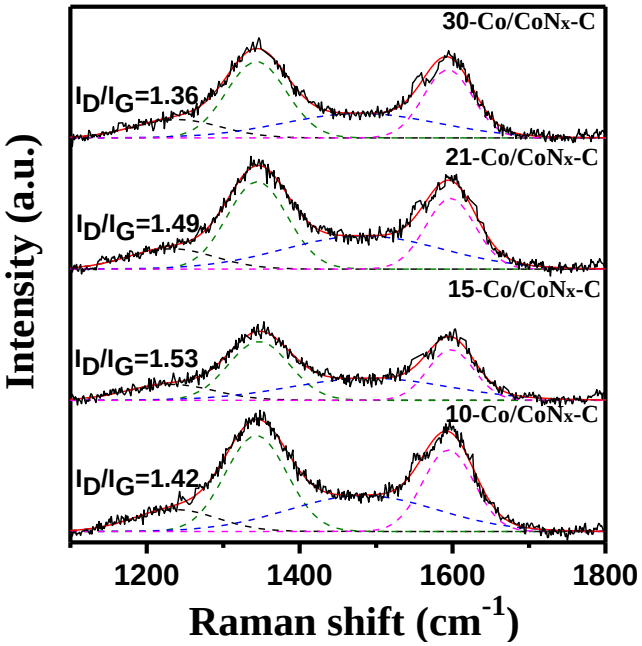

Figure S14. Raman spectra of Co/CoN$_x$-C catalysts.

The two typical peaks located in 1344 cm^{-1} (D band) and 1596 cm^{-1} (G band) stand for the disordered carbon (the defects) and sp^2 hybridization carbon species (graphitization).[1-3] The I_D/I_G values of electrocatalysts decreases from 1.53 (for 15-Co/CoNx-C) to 1.49 (21-Co/CoNx-C) and to 1.32 (30-Co/CoNx-C with large Co nanoparticles), meaning the high Co content results in the high graphitization degree during the calcination process (reduction of Co species to metallic Co clusters) to prepare the Co/CoN$_x$-C catalysts. The 15-Co/CoN$_x$-C catalysts with highest defect carbon level and disordered carbon matrix may promote the ORR performance.[1-3]

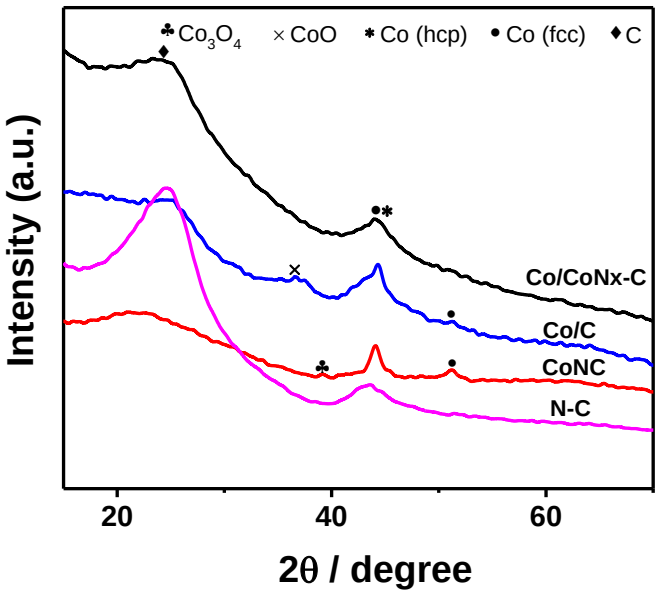

Figure S15. XRD patterns of 15-Co/CoN$_x$-C, 15-Co/C, 15-CoNC, and N-C catalysts. The diffraction lines at 36.7° (in Co/C) and 39.1° (in CoNC) were associated with the CoO (PDF#78-0431) and Co_3O_4 (PDF#42-1467).[4-6]

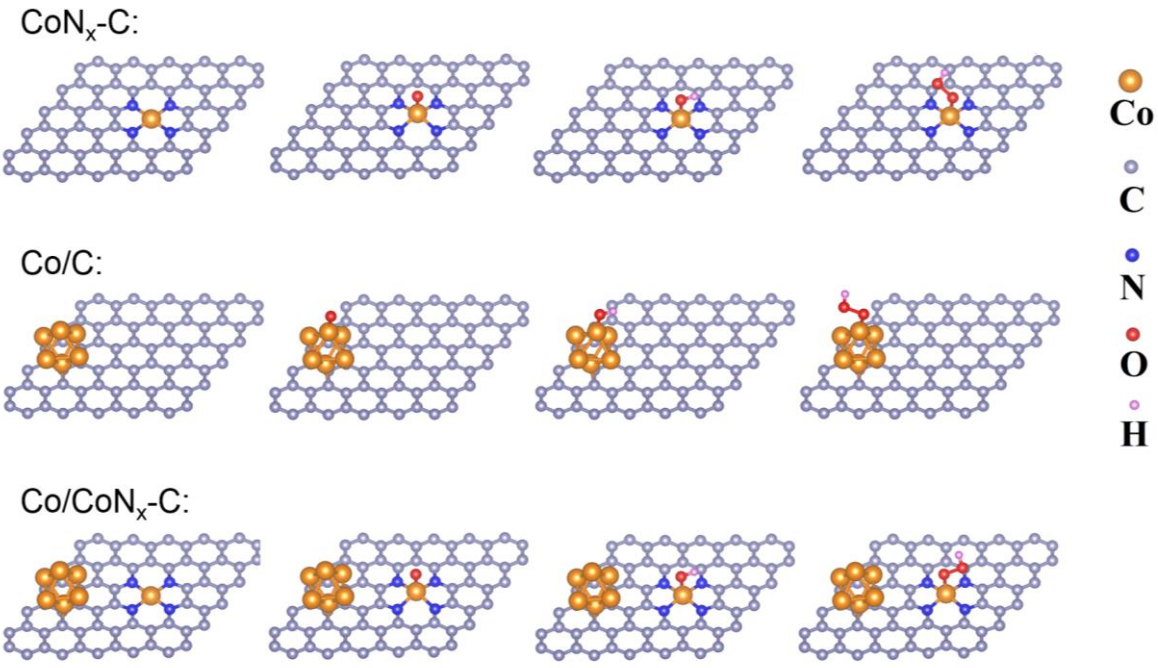

Figure S16. Oxygen reduction reaction pathway over CoN$_x$-C, Co/C, and Co/CoN$_x$-C electrocatalysts. Color code: Co orange; C, grey; N, blue; O, red; H, pink.

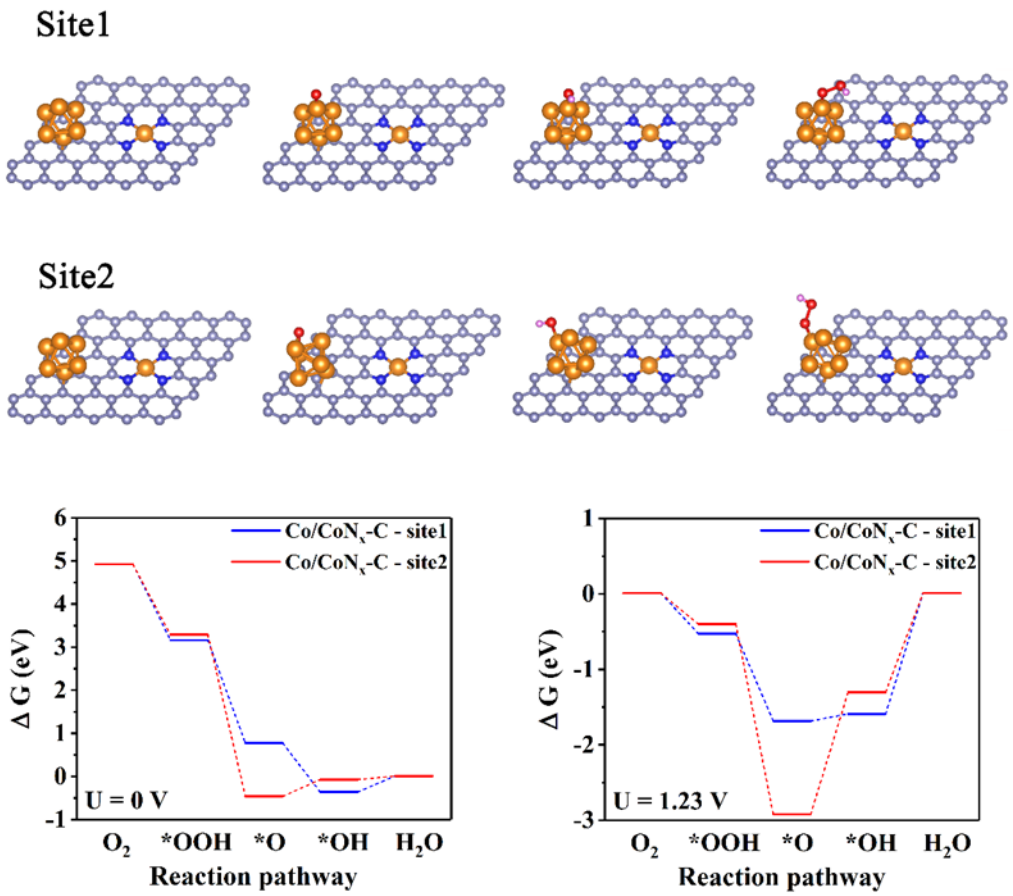

Figure S17. Oxygen reduction reaction pathway and free energy over the site1 and site2 on Co cluster of Co/CoN_x-C, respectively.

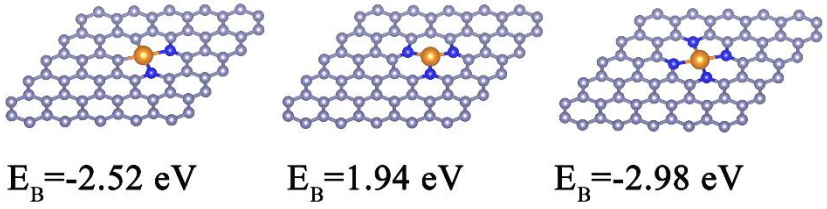

Figure S18. The binding energy of CoN_2, CoN_3, and CoN_4.

Table S1. The exact Co content in *x*-Co/CoN$_x$-C determined by TGA from Figure S1.

Catalyst	**10-Co/CoN$_x$-C**	**15-Co/CoN$_x$-C**	**21-Co/CoN$_x$-C**	**30-Co/CoN$_x$-C**
Co content (wt%)	10.1%	14.9%	21.2%	30.1%

Table S2. EXAFS fitting parameters at the Co K-edge for various samples (S_0^2=0.711).

Sample	**Shell**	**CN[a]**	**R (Å)[b]**	**σ ^{2} (Å^2)[c]**	**Δ E$_0$ (eV)[d]**	**R factor**
Co foil	Co-Co	12*	2.493± 0.002	0.0061± 0.0002	7.5	0.0010
15-Co/CoN$_x$-C	Co-Co	5.1±0.2	2.488± 0.002	0.0075± 0.0003	7.9	0.0006
	Co-N	2.6±0.6	1.978± 0.010	0.0147± 0.0038		

[a]CN, coordination number; [b]R, distance between absorber and backscatter atoms; [c]σ^2, Debye-Waller factor to account for both thermal and structural disorders; [d]ΔE_0, inner potential correction; R factor indicates the goodness of the fit. Note that the R value of 15-Co/CoN$_x$-C is calculated by phase correction.

Table S3. The fitting parameters of high-resolution XPS N 1s spectra of Co/CoN_x-C.

Binding energy of different types of N (eV) and content (%)					
Catalysts	**Pyridinic N**	**Co-N**	**Pyrrolic N**	**Graphitic N**	**Oxidized N**
10-Co/CoN_x-C	398.4 (21.2%)	399.1 (43.8%)	400.1 (15.9%)	401.0 (14.1%)	403.0 (5.0%)
15-Co/CoN_x-C	398.8 (24.8%)	399.4 (34.6%)	400.4 (19.3%)	401.4 (10.3%)	403.5 (11.0%)
21-Co/CoN_x-C	398.5 (22.2%)	399.1 (25.6%)	399.7 (23.5%)	401.0 (13.5%)	403.8 (15.2%)
30-Co/CoN_x-C	398.5 (41.2%)	399.5 (12.8%)	400.6 (23.8%)	401.4 (5.5%)	403.9 (16.7%)

Table S4. Comparison of ORR performances of 15-Co/CoN_x-C and presentative reported Co-based NNMEs in a O_2-saturated 0.1 M KOH solution in recent five years.

Catalyst	E_{onset} (V)	$E_{1/2}$ (V)	J_L (mA cm^{-2})	Ref.
NSC/Co_9S_8-200	0.93	0.83	5.98	[7]
CoS_x/NCNTs/Ni-2	--	0.79	5.6	[8]
Co_2/Fe-N@CHC	1.03	0.915	--	[9]
$Co(OH)_2$@NC	0.91	0.83	--	[10]
Co_3HITP_2	0.91	0.80	5.52	[11]
CoO_x/CoN_y@CN_2, 700	0.90	0.83	7.6	[12]
Co-Ni-SAS/NC	0.88	0.76	4.95	[13]
Co_3O_4/N-rGO	0.9	0.79	5.34	[14]
Co-N, B-CSs	0.89	0.83	5.66	[15]
CoNC-800	0.93	0.82	5.34	[16]
15-Co/CoN_x-C	0.926	0.853	6.20	***This work***

Reference

[1] Y. Q. Wang, K. Liu, J. Li, X. T. Yang, J. H. Hu, T. S. Chan, X. Q. Qiu, W. Z. Li and M. Liu, *Chem. Eng. J*., 2022, **429**, 132119.

[2] W. Q. Li, L. Wu, X. C. Wu, C. Shi, Y. L. Li, L. Zhang, H. W. Mi, Q. L. Zhang, C. X. He and X. Z. Ren, *Appl. Catal. B-Environ*., 2022, **303**, 120849.

[3] G. J. Li, Y. B. Tang, T. T. Fu, Y. Xiang, Z. P. Xiong, Y. J. Si, C. Z. Guo and Z. Q. Jiang, *Chem. Eng. J*., 2022, **429**, 132174.

[4] M. Sharma, J. H. Jang, D. Y. Shin, J. A. Kwon, D. H. Lim, D. Choi, H. Sung, J. Jang, S. Y. Lee, K. Y. Lee, H. Y. Park, N. Jung and S. J. Yoo, *Energy Environ. Sci*., 2019, **12**, 2200.

[5] K. Min, S. Kim, E. Lee, G. Yoo, H. C. Ham, S. E. Shim, D. Lim, S. H. Baeck, *J. Mater. Chem. A*, 2021, **9**, 17344.

[6] X. W. Zhong, W. D. Yi, Y. J. Qu, L. Z. Zhang, H. Y. Bai, Y. M. Zhu, J. Wan, S. Chen, M. Yang, L. Huang, M. Gu, H. Pan and B. M. Xu, *Appl. Catal. B-Environ*., 2020, **260**, 118188.

[7] Q. Zheng, Y. Xiong, K. Tang, M. Z. Wu, H. B. Hu, T. P. Zhou, Y. D. Wu, Z. Q. Cao, J. Sun, X. X. Yu and C. Z. Wu, *Nano Energy*, 2022, **92**, 106750.

[8] L. N. Lu, Y. L. Luo, H. J. Liu, Y. X. Chen, K. Xiao and Z. Q. Liu, *Chem. Eng. J*., 2022, **427**, 132041.

[9] Z. Wang, X. Jin, C. Zhu, Y. Liu, H. Tan, R. Ku, Y. Zhang, L. Zhou, Z. Liu, S.-J. Hwang and H. J. Fan, *Adv. Mater*., 2021, **33**, 2104718.

[10] Y. H. Zuo, M. J. Huang, W. C. Sheng, Q. Xu, W. Q. Tao and Z. Li, *Int. J. Hydrog. Energy*, 2022, **47**, 917.

[11] Y. B. Lian, W. J. Yang, C. F. Zhang, H. Sun, Z. Deng, W. J. Xu, L. Song, Z. W. Ouyang, Z. X. Wang, J. Guo and Y. Peng, *Angew. Chem. Int. Ed*., 2020, **59**, 286.

[12] J. Liu, C. Wang, H. Sun, H. Wang, F. Rong, L. He, Y. Lou, S. Zhang, Z. Zhang and M. Du, *Appl. Catal. B-Environ*., 2020, **279**, 119407.

[13] X. Han, X. Ling, D. Yu, D. Xie, L. Li, S. Peng, C. Zhong, N. Zhao, Y. Deng and W. Hu, *Adv. Mater*., 2019, **31**, 1905622.

[14] Y. Li, C. Zhong, J. Liu, X. Zeng, S. Qu, X. Han, Y. Deng, W. Hu and J. Lu, *Adv. Mater*., 2018, **30**, 1703657.

[15] Y. Guo, P. Yuan, J. Zhang, Y. Hu, I. S. Amiinu, X. Wang, J. Zhou, H. Xia, Z. Song, Q. Xu and S. Mu, *ACS Nano*, 2018, **12**, 1894.

[16] H. Jiang, Y. Liu, J. Hao, Y. Wang, W. Li and J. Li, *ACS Sustain. Chem. Eng*., 2017, **5**, 5341.